Available online at www.sciencedirect.com
SCIENCE DIRECT®
International Journal of Solids and Structures 41 (2004) 6429–6439
INTERNATIONAL JOURNAL OF SOLIDS and STRUCTURES
www.elsevier.com/locate/ijsolstr

Effective bending modulus of carbon nanotubes with rippling deformation

X. Wang *, Y.C. Zhang, X.H. Xia, C.H. Huang

Department of Engineering Mechanics, The School of Civil Engineering and Mechanics, Shanghai Jiaotong University, Shanghai 200240, People's Republic of China

Received 31 August 2003; received in revised form 20 April 2004
Available online 17 June 2004

Abstract

This paper concerned with the relation of the bending moment to the bending curvature during bending of carbon nanotubes, and the relation between the rippling formation and the bending modulus. Based on the three-dimensional orthotropic theory of finite elasticity deformation, a non-linear bending moment–curvature relationship of carbon nanotubes which is the appearance of wavelike distortion on the inner arc of the bent nanotubes is simulated by using an advanced finite element analysis package, *ABAQUS*. Utilizing the non-linear bending moment–curvature relationship, the effective bending modulus of carbon nanotubes with different cross-sections are obtained by means of a bi-linear theory and a simplified vibration analysis method. The effective bending modulus of carbon nanotubes simulated in the paper is close to the measuring result presented in reference [Science 283 (1999) 1513].

Keywords: Carbon nanotubes; Effective bending modulus; Non-linear-bending deformation; Ripple deformation

1. Introduction

Since their initial discovery by Iijima (1991), carbon nanotubes have come under ever increasing scientific scrutiny. The studies showed that carbon nanotubes exhibit superior mechanical properties over any known material. For instance, it was reported that carbon nanotubes appear in exceptionally high elastic modulus (higher than 1 TPa), and sustain large elastic strain (up to 5%) and breaking strain (up to 20%) (Iijima, 1991), they are also remarkably flexible in bending and can undergo large elastic deformation without breaking (Avouris et al., 1999; Dresselhaus et al., 2001; Yang et al., 2002). With these distinguishing properties, carbon nanotubes exhibit new phenomena, one of which is the formation of ripples when carbon nanotubes are under bending load (Treacy et al., 1996; Poncharal et al., 1999).

* Corresponding author. Tel./fax: +86-2154745367.
E-mail address: xwang@mail.sjtu.edu.cn (X. Wang).

0020-7683/$ - see front matter © 2004 Elsevier Ltd. All rights reserved.
doi:10.1016/j.ijsolstr.2004.04.038

Their potential applications have led to many investigations on measurements of mechanical properties of carbon nanotubes, by means of various techniques such as transmission electron microscopy (TEM) and atomic force microscopy (AFM). One good method of measurement used by Poncharal et al. (1999) is to measure the fundamental resonance included by an electric field in TEM and then calculate effective bending modulus E_{eff} by using the relation between resonance and modulus resulting from the linear vibration analysis of cantilevered beams. However, the result of measurement reported that the calculated effective bending modulus E_{eff} was found to decrease sharply, from about 1 to 0.1 TPa with the diameter D of carbon nanotubes increasing from 8 to 40 nm. This discovery defies usual belief that the elastic modulus is a material's intrinsic property, independent of the size of the nanotubes. Treacy et al. (1996) obtained an effective bending modulus E_{eff} of 1.8 TPa (average value) for multi-walled nanotubes, and Krishnan et al. (1998) obtained an effective bending modulus E_{eff} of 1.25 (−0.35/+0.45) TPa for single-walled nanotubes. Another approach is to use the tip of an AFM to bend anchored carbon nanotubes while simultaneously recording the force exerted by the tube as a function of the displacement from its equilibrium position. Then one can extract the effective bending modulus E_{eff} based on the elementary beam theory. Following this approach, Wong et al. (1997) obtained an effective bending modulus E_{eff} of 1.28 ± 0.5 TPa for multi-walled carbon nanotubes. It is a pity that all of the above measurements are indirect because the small dimension of nanotubes has made it extremely difficult to exactly measure their mechanical properties directly (Ebbesen, 1996). Thus it is also valuable to seek a numerical simulation method of obtaining the mechanical properties of carbon nanotubes.

A numerical simulation of materials of nanoscale size should use molecular dynamics (MD) method to consider the nanoeffects and to give an accurate solution. However, MD simulation is limited to systems with a maximum atom number of about 10^9 by the scale and cost of computation. So only single-walled nanotubes with small deflection can be simulated using MD method. Existing work shows that results from continuum mechanics agree with MD simulation results for single and double wall tubes. For examples, Yakobson et al. (1996) compared the results of atomistic modeling for axially compressed buckling of single-walled nanotubes with a simple continuum shell model, and found that all the buckling patterns displayed by MD simulation can also be predicted by the continuum shell model, and Antonio et al. (2004) presented some results demonstrate that the proposed continuum/FE technique could provide a valuable, easy-to-use and widely accessible tool for studying the mechanical behavior of carbon nanotubes. So FEM of a continuum model may be adopted to model molecular structures at the nanotube level.

Zheng and Jiang (2001) constructed a two-dimensional plane strain FEM model of a beam with rectangular across section under pure bending and obtained a bending moment–curvature relationship. But this model did not take into account the dimensional Poisson effect. Moreover, the material orientation of the model varies from carbon nanotubes, which are axially symmetric. A beam model with round cross-section of three dimensions have constructed, and a bending moment–curvature relationship, which is more likely to be the truly bending constitution of carbon nanotubes have obtained by using an advanced finite element analysis package, *ABAQUS*. Thus the effective bending moduli for carbon nanotubes with different cross-sections are obtained by means of using a bi-linear theory. The result carried out in the paper is consistent with the measuring result in reference (Poncharal et al., 1999).

2. Numerical simulation of rippling deformation mode

Based on three structures of carbon nanotubes arising from the folding of one layer or more layers of graphite to form a cylinder composed of carbon hexagons (Rao et al., 2001), we can utilize the stress–strain relationship of graphite to express the constitution of carbon nanotubes with an appropriate orientation. The experiments up to now do indicate that the axial elasticity modulus of carbon nanotubes is close to the

elasticity modulus along the basal plane of graphite (Krishnan et al., 1998). To better express the material's main direction of carbon nanotubes, the constitution in a cylindrical coordinate system is represented as

$$\begin{Bmatrix} \sigma_r \\ \sigma_\theta \\ \sigma_z \\ \tau_{\theta z} \\ \tau_{rz} \\ \tau_{r\theta} \end{Bmatrix} = 10^9 \times \begin{bmatrix} 36.5 & 15 & 15 & 0 & 0 & 0 \\ 15 & 1060 & 180 & 0 & 0 & 0 \\ 15 & 180 & 1060 & 0 & 0 & 0 \\ 0 & 0 & 0 & 220 & 0 & 0 \\ 0 & 0 & 0 & 0 & 2.25 & 0 \\ 0 & 0 & 0 & 0 & 0 & 2.25 \end{bmatrix} \begin{Bmatrix} \varepsilon_r \\ \varepsilon_\theta \\ \varepsilon_z \\ \gamma_{\theta z} \\ \gamma_{rz} \\ \gamma_{r\theta} \end{Bmatrix} \text{(Pa)} \tag{1}$$

In experiments the length-to-diameter ratio of carbon nanotubes is about 500. The loading condition is a concentrate force exerted at the free end of cantilever beam. The shearing effect for this kind of beam can be omitted based on solid mechanics theory, which belongs to purely bending model. Once the bending moment–curvature relationship for purely bending, which contains all the information of non-linearity, is obtained, the deformation and vibration of the cantilever beams can be analyzed without having to conduct an FEM simulation for each cantilever beam. Even so, because of the small size of elements aiming to characterize the rippling deformation, non-linear geometrical deformation and the time-consuming of computation, the length-to-diameter ratio should be kept to a suitable value. But there is a lowest limit, because the period of the rippling, namely, the length of each wave, is relation to the cross-sectional dimensions. This will vary to accommodate to ratio D/L, where D and L represent, respectively, the outer radius and the length of nanotubes, and affect the bending moment–curvature relationship. A ratio to contain enough waves in the deformation portion of beam should be determined, so that the length of the beam can be approximately taken as an integer multiple of the rippling period. Referring to the rippling period observed with high-resolution TEM (Poncharal et al., 1999) and the result of previous work (Zheng and Jiang, 2001), a rectangular cross-beam of length-to-height ratio L/h of 10:1 is chosen to simulate the rippling deformation of carbon nanotubes. In the paper it is assumed that carbon nanotubes with various inner radii d_i can be simulated using hollow cylindrical model or solid cylindrical model with the equative outer radius D.

The characteristic length of the bending portion of the beam between the two simply supported constraints is taken as L, and the bending curvature is taken as κ.

Using the same aspect ratio ($L/D = 500$) as that of experimental samples (Poncharal et al., 1999) to performing the finite element analysis is extremely challenging because the elements in finite element mesh must have dimensions significantly smaller than the spatial period of rippling. However, theoretically, under the pure bending condition the bending moment on each cross-section is the same and the beam's neutral axis has a constant curvature. Thus, a beam with smaller aspect ratio ($L/D \ll 500$) can be used to simulate the rippling deformation of the beam under the pure bending condition. It should be pointed out that in the FEM numerical simulation the exact application of the boundary condition of the beam subjected to pure bending is very important, due to the rotation and the changing unknown stress distribution of the ending sections. An approach is to construct a four-point bending beam, as shown in Fig. 1.

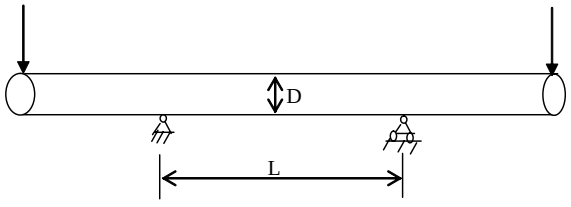

Fig. 1. Three-dimensional FEM calculating models for purely bending nanotubes.

A commercial finite element code *ABAQUS* is used to simulate the rippling formation of bent nanotubes. It can automatically choose proper loading increments and converge criteria in a non-linear analysis.

Fig. 2(a) shows the undeformed mesh of solid cylindrical model for carbon nanotubes, Fig. 2(b) shows the configuration of a simulated this carbon nanotubes bent with the rippling deformation which is similar to overall view of a bending carbon nanotubes with ripples carried out by means of a measuring method (Poncharal et al., 1999).

In order to minimize the sensitivity of numerical solution to the characteristic length of the selected purely bending portion by varying the aspect ratio we plot in Fig. 3 the bending moment M versus the bending curvature κ at each loading step for the four-point bending solid cylinder with the length-to-diameter ratios $L/D = 10$, and 20. It is seen from Fig. 3 that the calculating results for the two different dimensions of purely bending portion of the four-point bending solid cylinder models are approximate coincidence so that in the following finite element simulation the length-to-diameter ratios L/D of purely bending portion may be taken as 10 in order to decrease the calculating time.

From Fig. 3, it is seen that the bending stiffness of a carbon nanotube sharply reduces from the EI value as it is bent into the rippling mode. Because the reduced bending stiffness doses not change significantly, the bending moment–curvature relationship can be simplified as a bi-linear function.

Fitting the discrete data in Fig. 3 with bi-linear functions gives

$$M = \begin{cases} EI\kappa & \text{as } 0 \leqslant \kappa \leqslant 1.36\% \\ e_1 EI\kappa + e_2 & \text{as } \kappa > 1.36\% \end{cases} \tag{2a}$$

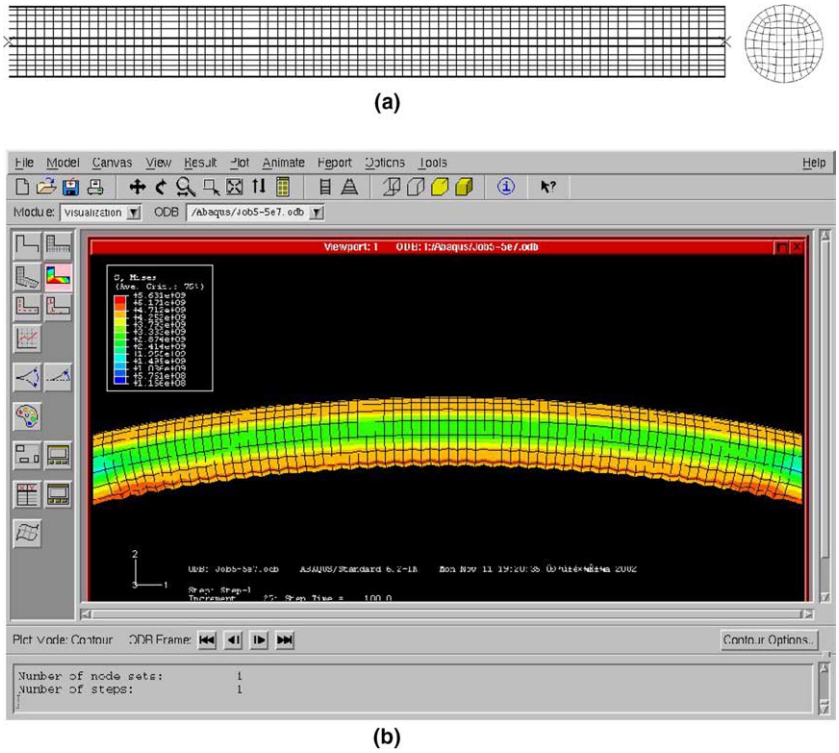

Fig. 2. FEM model of carbon nanotubes and the rippling configuration. (a) The undeformed mesh of the purely bending part, (b) The rippling deformed shape of the bent carbon nanotubes from FEM simulation.

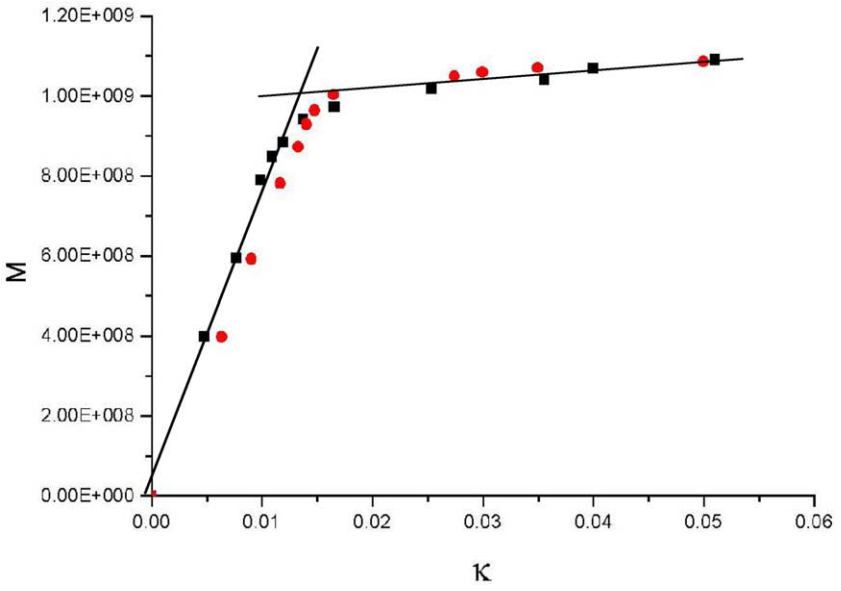

Fig. 3. Two results derived from different ratios to D/L, where (■) represents $L/D = 10$, (●) represents $L/D = 20$.

with $e_1 = 0.0684$, $e_2 = 0.898 \times 10^9$ Nm, where $E = 1.02 \times 1012$ GPa is the axial engineering elastic constant derived from the Young's modulus of the graphite base plane.

In fact, the dimensionless curvature $D\kappa$ has an obvious physical meaning which expresses two times the maximum normal strain ε_{max} when the beam is bent in the linear mode. So, when non-linear mode appear the above function gives the critical strain

$$\varepsilon_{cr} = 0.0136D/2 \tag{2b}$$

3. A bending experiment method of nanotubes

Based on that all the electrostatic force is exerted at the free end of the carbon nanotubes (Poncharal et al., 1999), the load applied on the cantilever beam is written as

$$F(x,t) = P(t)\delta(x - L) \tag{3}$$

where a concentrate force $P(t)$ is exerted at the location $x = L$.

Because the surface work function of carbon nanotubes is different from that of the counter electrode, they will interact and bear a certain amount of static charge even when no voltage is applied between the carbon nanotubes and the counter electrode. Suppose the net charge of carbon nanotubes is q_0, which neutralizes the difference of the surface work function. This net charge can be eliminated by applying a bias voltage $-\Delta V$, with $\Delta V = q_0/\alpha$, where α is the proportional constant between the induced charge (with the exclusion of q_0) and the applied voltage. When a time dependent voltage $V(t) = V_s + V_d \cos(\omega t)$ is applied, the charge at the free end of the carbon nanotubes is $q = q_0 + \alpha V(t) = \alpha[\Delta V + V(t)]$, and the intensity of the electric field there is $E = \beta[\Delta V + V(t)]$, so the electric force exerted on the carbon nanotubes is $P(t) = Eq = \alpha\beta[\Delta V + V(t)]^2$, where α and β are proportional constants relevant to the carbon nanotubes under investigation. Substituting the expression of $V(t)$ into that function, gives

$$P(t) = \alpha\beta[\Delta V + V_s + V_d\cos(\omega t)]^2$$
$$= \alpha\beta[(\Delta V + V_s)^2 + 2(\Delta V + V_s)V_d\cos(\omega t) + (1/2)V_d^2\cos(2\omega t) + (1/2)V_d^2] \quad (4)$$

From the above expression, it can be seen that static load P_0 and periodical load $P_1(t)$ in Eq. (4) are, respectively, expressed as

$$P_0 = \alpha\beta[(\Delta V + V_s)^2 + (1/2)V_d^2] \quad (5a)$$

$$P_1(t) = \alpha\beta[2(\Delta V + V_s)V_d\cos(\omega t) + (1/2)V_d 2\cos(2\omega t)] \quad (5b)$$

In a linear vibration the stimulation with frequency being ω and 2ω in $P_1(t)$ are analyzed respectively, and their response are superimposed. Since $(\Delta V + V_s)/V_d \gg 1$ in the experiment, there are

$$P_0 \approx \alpha\beta[(\Delta V + V_s)^2] \quad (6a)$$

$$P_1(t) \approx \alpha\beta[2(\Delta V + V_s)V_d\cos(\omega t)] \quad (6b)$$

where $P_0 \gg P_1(t)$.

The beam undergoes a static deformation of bending when P_0 is exerted on it, and part of the beam has entered the rippling mode. $P_1(t)$ cause the beam to vibrate. Suppose that the interface between the rippling and un-rippling parts is at $x = L_1$, where L_1 is determined by

$$\varepsilon_{max} = \frac{D}{2}\frac{P_0(L - L_1)}{EI} = \varepsilon_{cr} \quad (7)$$

where D expresses the diameter of carbon nanotubes, and the critical strain ε_{cr} for rippling is given in Eq. (2b). Solving Eq. (7) gives

$$L_1 = L - \frac{2\varepsilon_{cr}EI}{DP_0} \quad (8a)$$

$$L_2 = \frac{2\varepsilon_{cr}EI}{DP_0} \quad (8b)$$

where $L_2 = L - L_1$.

The rippling part of the beam appears in $0 \leqslant x \leqslant L_1$, and the un-rippling part appears in $L_1 < x \leqslant L$. These two parts will observe $\frac{dM}{d\kappa} = e_1 EI$ and $\frac{dM}{d\kappa} = EI$ respectively. Because $P_1(t)$ cause the whole beam to vibrate, the interface between the two parts oscillates around $x = L_1$, which means that the lengths of the two parts appears in fluctuating. However, because the dynamic deformation is small compare to the static deformation, and the effects of positive fluctuation and negative fluctuation in a period on the frequency of vibration can counteract to some extent, the vibration analysis for a beam with two parts of constant lengths having different bending stiffness can be adopted.

According to the experiment (Poncharal et al., 1999), it is assumed that the ratio of the displacement of the free end of the cantilever beam caused by P_0 (w_{max}) to the beam length L is a constant

$$\frac{w_{max}}{L} = C_F \quad (9)$$

Considering that C_F approximately equals 30% (Poncharal et al., 1999) and from material's mechanics theory the displacement of the free end of the cantilever beam is given by

$$w_{max} = \frac{P_0}{EI}\left[\frac{1}{\alpha_1}\left(\frac{L_1^3}{3} + L_1^2 L_2 + L_1 L_2^2\right) + \frac{L_2^3}{3}\right] \quad (10)$$

Solving Eq. (7) yields

$$P_0 = \frac{2EI\varepsilon_{cr}}{DL_2} \tag{11}$$

Substituting Eq. (1) into Eq. (10), and dividing both sides of the equation by L, gives

$$\begin{aligned}\frac{w_{max}}{L} &= \frac{2\varepsilon_{cr}}{DL}\left[\frac{1}{e_1}\left(\frac{L_1^3}{3L_2}+L_1^2+L_1L_2\right)+\frac{L_2^2}{3}\right] = \frac{2\varepsilon_{cr}}{D/L}\left[\frac{1}{e_1}\left(\frac{L_1^3}{3L_2L^2}+\frac{L_1^2}{L^2}+\frac{L_1L_2}{L^2}\right)+\frac{L_2^2}{3L^2}\right]\\ &= \frac{2\varepsilon_{cr}}{D/L}\left[\frac{1}{e_1}\left(\frac{k^3}{3(1-k)}+k^2+k(1-k)\right)+\frac{(1-k)^2}{3}\right] = \frac{2\varepsilon_{cr}}{D/L}\frac{k^3 3k^2+3k+\alpha_1(1-k)^3}{3e_1(1-k)} = C_F\end{aligned} \tag{12}$$

where $\frac{L_2}{L_1} = \frac{1-k}{k}$.

The above equation indicates that the quotient of the rippling part in the model $k = L_1/L$ is only determined by the geometric parameter of the beam D/L. Once the value of D/L is given, k in the above equation can be easily obtained.

4. Bending vibration theory of beam

According to the bi-linear constitution relationship simulated shown in Fig. 3 and the vibration theory of beam the bending vibration equation of beam is separated into two parts

$$e_1EI\frac{\partial^4 w_1(x,t)}{\partial^4 x}+\rho A\frac{\partial^2 w_1(x,t)}{\partial^2 t}=0 \quad (0\leqslant x\leqslant L_1) \tag{13a}$$

$$EI\frac{\partial^4 w_2(x,t)}{\partial^4 x}+\rho A\frac{\partial^2 w_2(x,t)}{\partial^2 t}=P_1(t)\delta(x-L) \quad (L_1\leqslant x\leqslant L) \tag{13b}$$

where subscriptions 1 and 2 represent the bending equilibrium equations of the rippling and un-rippling parts of the beam. Boundary conditions and continuous conditions of the cantilever beam are, respectively,

$$w_1 = \partial w_1/\partial x = 0, \quad \text{at } x = 0$$

$$\frac{\partial^2 w_2}{\partial^2 x} = \frac{\partial^3 w_2}{\partial^3 x} = 0, \quad \text{at } x = L$$

$$w_1 = w_2, \quad \partial w_1/\partial x = \partial w_2/\partial x$$

$$\frac{\partial^2 w_1}{\partial^2 x} = \frac{\partial^2 w_2}{\partial^2 x}, \quad \frac{\partial^3 w_1}{\partial^3 x} = \frac{\partial^3 w_2}{\partial^3 x}, \quad \text{at } x = L_1 \tag{14}$$

Assuming the homogeneous solutions of Eq. (13) are, respectively, written as

$$w_1(x,t) = \phi_1(x)q_1(t) \quad (0\leqslant x\leqslant L_1) \tag{15a}$$

$$w_2(x,t) = \phi_2(x)q_2(t) \quad (L\leqslant x\leqslant L) \tag{15b}$$

where

$$\phi_1(x) = C_1\sinh(\beta_1 x)+C_2\cosh(\beta_1 x)+C_3\cos(\beta_1 x)+C_4\sin(\beta_1 x) \tag{16}$$

expresses the mode function of rippling deformation, and

$$\phi_2(x) = C_5\sinh(\beta_2 x)+C_6\cosh(\beta_2 x)+C_7\cos(\beta_2 x)+C_8\sin(\beta_2 x) \tag{17}$$

expresses the mode function of non-rippling deformation. In the above formula,

$$\beta_1 = \sqrt[4]{\frac{\rho A}{e_1 EI}\omega^2}, \quad \beta_2 = \sqrt[4]{\frac{\rho A}{EI}\omega^2} \tag{18}$$

Assume that a new coordinate system is expressed as

$$x_1 = x \quad (0 \leqslant x \leqslant L_1 \text{ and } 0 \leqslant x_1 \leqslant L_1)$$

$$x_2 = x - L_1 \quad (L_1 \leqslant x \leqslant L \text{ and } 0 \leqslant x_2 \leqslant L_2) \tag{19}$$

Under the coordinate system (19), and substituting Eq. (15) into the boundary condition and the continuous condition (14) yields

$$\begin{aligned} &\phi_1(L_1) = \phi_2(0), \quad \phi_1'(L_1) = \phi'(0)_2 \\ &e_1\phi_1''(L_1) = \phi_2''(0), \quad e_1\phi_1'''(L_1) = \phi_2'''(0) \\ &\phi_1(0) = \phi_1'(0) = 0, \quad \phi_2''(L_2) = \phi_2'''(L_2) = 0 \end{aligned} \tag{20}$$

Substituting Eqs. (16) and (17) into Eq. (20) leads to a set of algebraic equations.

$$\begin{cases} C_2 + C_3 = 0 \\ C_1 + C_4 = 0 \\ C_5 \mathrm{sh}\,\beta_2 L_2 + C_6 \mathrm{ch}\,\beta_2 L_2 - C_7 \cos\beta_2 L_2 - C_8 \sin\beta_2 L_2 = 0 \\ C_5 \mathrm{ch}\,\beta_2 L_2 + C_6 \mathrm{sh}\,\beta_2 L_2 + C_7 \sin\beta_2 L_2 - C_8 \cos\beta_2 L_2 = 0 \\ C_1 \mathrm{sh}\,\beta_1 L_1 + C_2 \mathrm{ch}\,\beta_1 L_1 + C_3 \cos\beta_1 L_1 + C_4 \sin\beta_1 L_1 = C_6 + C_7 \\ \beta_1(C_1 \mathrm{ch}\,\beta_1 L_1 + C_2 \mathrm{sh}\,\beta_1 L_1 - C_3 \sin\beta_1 L_1 + C_4 \cos\beta_1 L_1) = \beta_2(C_5 + C_8) \\ e_1\beta_1^2(C_1 \mathrm{sh}\,\beta_1 L_1 + C_2 \mathrm{ch}\,\beta_1 L_1 - C_3 \cos\beta_1 L_1 - C_4 \sin\beta_1 L_1) = \beta_2^2(C_6 - C_7) \\ e_1\beta_1^3(C_1 \mathrm{ch}\,\beta_1 L_1 + C_2 \mathrm{sh}\,\beta_1 L_1 + C_3 \sin\beta_1 L_1 - C_4 \cos\beta_1 L_1) = \beta_2^3(C_5 - C_8) \end{cases} \tag{21}$$

In order to get non-zero solutions for the above equation, making the coefficient matrix of Eq. (21) be zero, gives

$$\begin{aligned} &[\cosh(X)\cosh(X) - 1][\cosh(Y)\cos(Y) - 1] + e_1[\cosh(X)\cosh(X) + 1][\cosh(Y)\cos(Y) + 1] \\ &+ e_1^{\frac{3}{4}}[\cosh(Y)\sin(Y) + \sinh(Y)\cos(Y)][\sinh(X)\cos(X) - \cosh(X)\sin(X)] + e_1^{\frac{1}{4}}[\cosh(X)\sin(X) \\ &+ \sinh(X)\cos(X)][\sinh(Y)\cos(Y) - \cosh(Y)\sin(Y)] - 2e_1^{\frac{1}{2}}\sinh(X)\sin(X)\sinh(Y)\sin(Y) \\ &= 0 \end{aligned} \tag{22}$$

where $X = \beta_1 L_1$, $Y = \beta_2 L_2$. It is noted that Eq. (22) involves two dimensionless undetermined parameters, X and Y. From Eq. (8) and Eq. (18) we have

$$X = \frac{\beta_1 L_1}{\beta_2 L_2} = \frac{3C_F D/L - 2\varepsilon_{cr}}{2\varepsilon_{cr} e_1^{1/4}} Y \tag{23}$$

Substituting Eq. (23) into Eq. (22), the minimum real root of Eq. (22) is given by

$$Y_1 = \beta_{21} L_2 \tag{24}$$

Substituting β_{21} into Eq. (18), the basic frequency of the cantilever beam is written as

$$\omega_1 = \beta_{21}^2 \sqrt{\frac{E_{eff} I}{\rho A}} = \frac{Y_1^2}{L_2^2} \sqrt{\frac{E_{eff} I}{\rho A}} \tag{25}$$

where E_{eff} expresses an equivalent bending modulus.

From a linear vibration theory, the basic frequency of the cantilever beam may be written as

$$\omega_1^l = \frac{(\beta_1^l L)^2}{L^2}\sqrt{\frac{EI}{\rho A}} = \frac{1.875^2}{L^2}\sqrt{\frac{EI}{\rho A}} \tag{26}$$

where $\beta_1 L$ is the minimum real root of the characteristic equation which is expressed as

$$\cos(\beta_1 L)\cosh(\beta_1 L) + 1 = 0 \tag{27}$$

Using Eqs. (25) and (26), we have

$$\frac{E_{\text{eff}}}{E}\left(\frac{\omega_1}{\omega_1^l}\right)^2 = \left(\frac{Y_1}{1.875}\frac{3C_F D/L}{2\varepsilon_{\text{cr}}}\right)^4 \tag{28}$$

From Eqs. (8a) and (2b), when non-rippling deformation appears on the beam ($L_1 = 0$), we have

$$D/L = \frac{2\varepsilon_{\text{cr}}}{3C_F} = \frac{2 \times 0.0136 D/2}{3 \times 30\%} = 0.0151D \tag{29}$$

When $D/L < 0.0151D$, the beam completely appears in the linear M–κ relationship. Substituting a series of values $D/L > 0.0151D$ into Eq. (22) gives the relation between the effective modulus E_{eff} and D/L shown as the curve A in Fig. 4.

On the other hand, utilizing Microcal Origin Code, we simulate the curve A in Fig. 4 with a simple function describing relationship between the effective modulus E_{eff} and D/L when rippling deformation appear on the bending beam, which is given by

$$\frac{E_{\text{eff}}}{E} = 0.05949 + \frac{5 \times 10^{-5}}{\left(\frac{D}{L} - 0.01305\right)^{1.21684}} \tag{30}$$

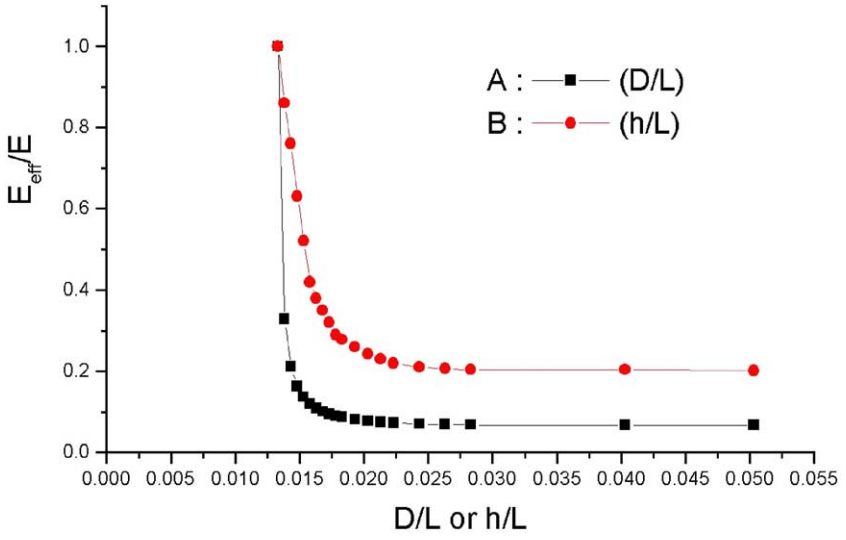

Fig. 4. Curve A expresses the relationship between diameter-to-length D/L and effective bending modulus E_{eff}/E of carbon nanotubes from three-dimension solid circle section model. Curve B expresses the relationship between height-to-length h/L and effective bending modulus E_{eff}/E of carbon nanotubes from two-dimension rectangular section beam.

5. Conclusions

From the curve A in Fig. 4, it is seen that when the length of the carbon nanotubes is a constant, its effective bending modulus carried out according to the bi-linear deformation theory does decrease with the diameter of the carbon nanotubes increasing. The distribution of the data points from the curve A in Fig. 4 is closed to that of the $E_{\text{eff}}/E - D$ graph derived from experiment in reference (Poncharal et al., 1999).

Fig. 4 shows a comparison between the $E_{\text{eff}}/E - D/L$ relationship in this paper and the result from the FEM model of which is a square-cross-sectioned beam with the height being h in reference (Zheng and Jiang, 2001). In the comparison, to make the cross-sections of the two models have an equal inertial moment a value to the diameter of circle-sectioned beam in the paper is given by

$$\frac{\pi D^4}{64} = \frac{bh^3}{12} \tag{31}$$

It is seen from Fig. 4 that although the two curves are similar, the result in this paper gives a lower value for E_{eff}/E with D/L increasing, which is more closer the $E_{\text{eff}}/E - D$ graph derived from experiment (Poncharal et al., 1999) than the two-dimensional model (Zheng and Jiang, 2001). Thus, it is concluded that the three-dimensional model used in this paper is more suitable to simulate the effective bending modulus of carbon nanotubes with rippling deformation than the two-dimensional model in reference (Zheng and Jiang, 2001).

In order to further describe the effect of FEM model on numerical simulation of the effective bending modulus of carbon nanotubes with rippling deformation, a hollow circle section is used to simulate the effective bending modulus of carbon nanotubes with rippling deformation. Similar to Eq. (31), the geometrical sizes of hollow circle section is given by

$$D_1^4 - d^4 = D^4 \tag{32}$$

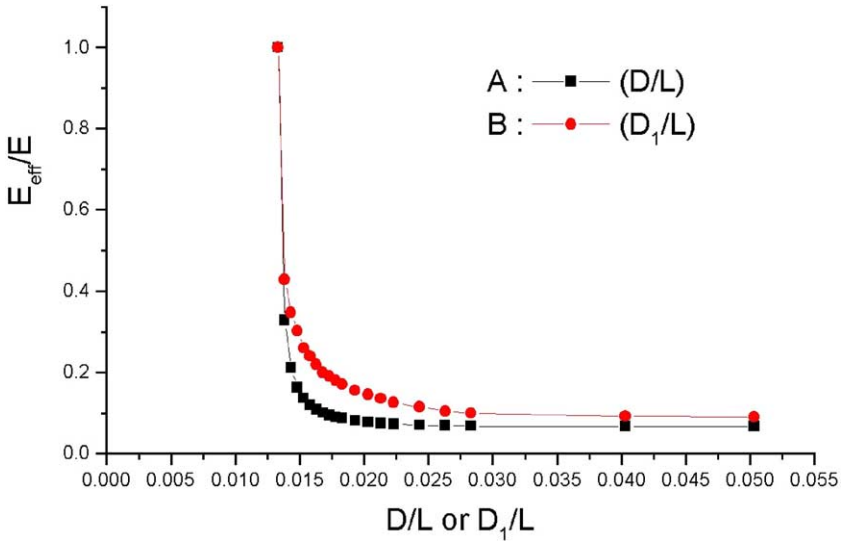

Fig. 5. Curve A expresses the relationship between diameter-to-length D/L and effective bending modulus E_{eff}/E of carbon nanotubes from three-dimension solid circle section model. Curve B expresses the relationship between height-to-length h/L and effective bending modulus E_{eff}/E of carbon nanotubes from three-dimension hollow circle section model.

where D presents the outer radii of the solid circle section, D_1 presents the out radii of the hollow circle section and $d = D_1/2$ presents the internal radii of the hollow circle section.

Fig. 5 shows the distributions of the effective bending modulus of carbon nanotubes with rippling deformation for two kinds of sections model with identical dimensions and inertial moment. It is seen that the distributions of the two effective bending moduli of carbon nanotubes with rippling are approach. It further proves that the circle section used to simulate the effective bending modulus of carbon nanotubes is suitable.

Acknowledgement

The authors thank the referees for their valuable comments.

References

Antonio, P., David, M.P., Mary, C.B., 2004. Mechanics of deformation of single- and multi-wall carbon nanotubes. J. Mech. Phys. Solids 52, 789–821.

Avouris, P.H., Hertel, T., Martel, R., Schmidt, T., Shea, H.R., Walkup, R.E., 1999. Carbon nanotubes: nanomechanics, manipulation, and electronic devices. Appl. Surf. Sci. 141, 201–209.

Dresselhaus, M.S., Dresselhaus, G., Avouris, P.H., 2001. Carbon nanotubes. Topics Appl. Phys. 80, 287–329.

Ebbesen, T.W., 1996. Phys. Today 49 (6), 26.

Iijima, S., 1991. Helical microtubes of graphitic carbon. Nature 354, 56–58.

Krishnan, A., Dujardin, E., Ebbesen, T.W., Yianilos, P.N., Treacy, M.M.J., 1998. Phys. Rev. B 58, 14013.

Poncharal, P., Wang, Z.L., Ugarte, D., de Heer, W.A., 1999. Electrostatic deflections and electromechanical resonances of carbon nanotubes. Science 283, 1513–1516.

Rao, C.N.R., Satishkumar, B.C., Govindaraj, A., Nath, M., 2001. Chemphyschem 2, 78–105.

Treacy, M.M.J., Ebbesen, T.W., Gibson, J.M., 1996. Nature 381, 678.

Wong, E.W., Sheehan, P.E., Liebert, C.M., 1997. Science 277, 1971.

Yakobson, B.I., Brabec, C.J., Bernholc, J., 1996. Rev. Lett. 76, 2511–2514.

Yang, W. et al., 2002. Advances in nanomechanics. Adv. Mech. 32, 161–174.

Zheng, Q.S., Jiang, Q., 2001. Effect of rippling mode to resonances of carbon nanotubes. In: Proceeding of the International Symposium on Mechanics and Material Engineering. August, Changsha, China, pp. 13–17.